Study on Seepage and Mass Transfer Characteristics During CO_2 Storage in Saline Aquifer

Weixin Zhang, Bohao Wu, Pengfei Lv, Shaohua Li, and Lanlan Jiang(✉)

Key Laboratory of Ocean Energy Utilization and Energy Conservation of Ministry of Education, Dalian University of Technology, Dalian 116024, China

lanlan@dlut.edu.cn

Abstract. CO_2 storage in saline aquifer is considered to be the most potential and most promising method to alleviate greenhouse effect and neutralize CO_2. Rock wettability and heterogeneity study is crucial for CO_2 storage in saline aquifer due to the complex geological structure of submarine surroundings. In this study, CO_2 dynamic displacement process and imbibition process in sand cores were captured by CT scanning technology in different conditions (40 °C, 8 Mpa and 25 °C, 0.1 Mpa). Experiment result shows that stronger wettability is conducive to the occurrence of CO_2 snap off and increases the safety of CO_2 capillary capture and storage, while imbibition of weaker wettability porous media is more stable but CO_2 is difficult to capture. Moreover, CO_2-salt water interface was divided into three categories (interface aggregation nodes, interface clusters and interface monomers) and interface evolution low was quantified by the liner relationship of relative interface area (*RIA*) and salt water saturation (*Sw*). Upward imbibition is beneficial for CO_2 storage according to the *RIA* of the upward imbibition process is about 1.3 times that of downward when salt water saturation keeps the same. Finally, the heterogeneity of the mixed sand significantly increases the contact area of the two phases than uniform sand for the same Reynolds number. The microscopic transport mechanism and morphological distribution characteristics of CO_2-salt water in the pores in this paper has some implication for practical CO_2 long-term and safe storage in saline aquifer.

Keywords: CO_2 storage · CT · Wettability · Interface between two phases

Symbol Description

Sw	salt water saturation
RIA	relative interface area
PV	pore volume
a_i	specific interface area

© The Author(s), under exclusive license to Springer Nature Singapore Pte Ltd. 2022
B. Sun et al. (Eds.): DWOG-Hyd 2021, LNCE 246, pp. 210–220, 2022.
https://doi.org/10.1007/978-981-19-0960-3_21

1 Introduction

CO_2 reduction and CO_2 neutralization have become the consensus of more and more people. CO_2 storage in saline aquifer has enormous potential to significantly slow the pace of global climate change by bury massive CO_2 in deep saline aquifers.

The storage efficiency of storage CO_2 largely depends on the properties of the target reservoir rock [1–3]. Rock wettability and heterogeneity study is crucial for CO_2 storage in saline aquifer due to the diverse composition of rock and the complex geological structure of submarine surroundings. As a non-invasive technology, X-ray CT imaging can generate three-dimensional pore-scale images with micro-level spatial resolution, which is critical for visualizing mass transfer process. Gao [4] studied the characteristics of Estaillades carbonate rock, which is different from previous sandstone studies and found that it has complex heterogeneity. Brusseau [5] studied the interface distribution in different types of porous media and found that the specific interface area and the maximum specific interface area are inversely proportional to the median particle size of the porous media.

Moreover, the CO_2-salt water interface is the main area of mass transfer between each phase during the storage process. To better understand the CO_2 dissolution process and CO_2-salt water mass transfer in the pores, it is necessary to study the evolution law of the CO_2-salt water interface. For the interface between phases in two-dimensional porous media, the interface area between phases can be directly measured by the displacement experiment in the micro-etched glass plate of the porous media [6, 7]. Jettestuen et al. simulated the process of imbibition in a three-dimensional sandstone, and observed the retraction of the interphase interface into the pores, the expansion of the wetting phase film and the snap-off effect [8]. The interface plays a vital role in the mass transfer process of each phase, but this time-varying process lacks sufficient quantitative analysis [9].

We have established a set of experimental methods based on the microfocus X-ray CT system to measure the mass transfer of CO_2 under complex conditions of multi-components. Using CT continuous scanning to obtain the microscopic pore structure of the sand-filled sample and the dynamic evolution process of the CO_2-salt-water interface. Then with the help of image processing technology, we explored the impact of the wettability and heterogeneity of different reservoir components on CO_2 storage. In addition, we studied the changes of the CO_2-brine phase interface under different salt water injection flow rates, that realizing the dynamic visualization of the CO_2-salt water interface. The microscopic transport mechanism and morphological distribution characteristics of CO2-salt water in this paper has some implication for practical CO_2 long-term and safe storage in saline aquifer [10, 11].

2 Experimental Method

2.1 Materials and Setup

Figure 1 is a diagram of the microscopic visualization test system of CO_2-salt water mass transfer characteristics. The experimental system is mainly composed of three parts: micro-focus X-ray CT visual imager (resolution is 4 μm), injection and recovery system, and temperature and pressure control system. In the reactor used in this experiment, the

part of the tube wall through which X-rays penetrate is made of polyether ether ketone (PEEK), which ensures the quality of CT imaging while minimizing the attenuation of X-rays [12]. ISCO piston pumps are used in the experiment as the gas injection, water injection and pressure control system. A circulating temperature controller is used to control the temperature of the injected fluid to simulate the environment of the porous medium of the saline aquifer reservoir. Finally, we use high-precision pressure sensors and thermocouples to monitor and automatically collect the temperature and pressure data of the system.

In the filled sandstone core, artificial glass sand with different particle sizes (produced by Japan's AS-ONE company) and natural quartz sand, dolomite and feldspar sand (purchased from Hebei sand quarry) were used. The shape of glass sand is a relatively regular sphere, while the shapes of quartz sand, dolomite and feldspar sand are irregular. The mineral composition of each sand is single, and its specific particle size distribution is shown in Table 1. During the process of filling the core, a combination of multiple filling layer by layer and several shaking by percussing is used, which can not only avoid delamination during the filling process, but also ensure that the sand core is compacted well. Then graphite electric heating tape is used to heat it up to the experimental temperature. For the experiment, the gas used is high-purity CO_2 with a purity of 99.9% and the salt water is made up of deionized water and 3% sodium chloride (Analytical Pure AR, Tianjin Komiou Chemical Reagent Co., Ltd.) to simulate the salinity of saline water in underground reservoirs. In addition, potassium iodide with a mass fraction of 6% is added as a contrast agent to enhance the contrast between gas and salt water in CT images.

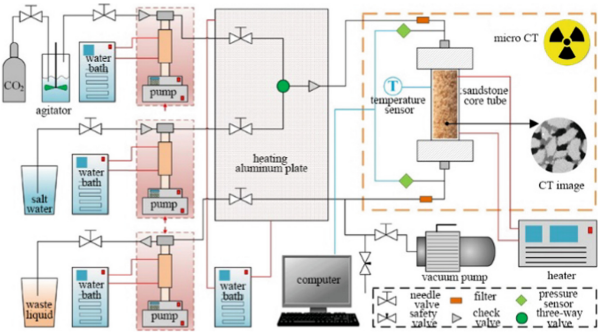

Fig. 1. Schematic diagram of experimental device

2.2 Experimental Approach

(1) Preparation of porous medium and two-phase fluid: placing the porous medium into the reactor before the experiment, and then connecting the experimental pipeline according to Fig. 1. High-pressure gas is used to clean the pipeline and leak detection to ensure that there is no liquid residue in the pipeline. Before each experiment starts, vacuuming for 20 min to remove the gas. A sodium chloride solution with a mass

Table 1. Types and detailed parameters of sand used in the experiment.

Sand type	Particle size/mm	Average particle size/mm
Glass sand BZ06	0.500–0.710	0.6
Glass sand BZ04	0.350–0.500	0.4
Glass sand BZ02	0.177–0.250	0.2
Rough quartz sand	0.355–0.425	0.4
Fine quartz sand	0.180–0.212	0.2
Rough feldspar	0.355–0.425	0.4
Fine feldspar	0.180–0.212	0.2
Rough dolomite	0.355–0.425	0.4
Fine dolomite	0.180–0.212	0.2

Table 2. CO_2 saturation of each layer after the displacement process of layered sand filling core.

Rock stratum	SCO_2 (40 °C, 8 MPa)		SCO_2(25 °C, 101 kPa)	
	0.1 mL/min	0.3 mL/min	0.6 mL/min	0.3 mL/min
BZ06	0.80	0.81	0.80	0.78
BZ02	0.18	0.10	0.06	0.07
Quartz	0.14	0.07	0.06	0.12
Dolomite	0.74	0.55	0.24	0.29

fraction of 3% is prepared, and potassium iodide with a mass fraction of 6% is added as a contrast agent.

(2) Displacement process: after vacuuming, the sand-filled core is injected with salt water through the liquid injection pump. The pressure and temperature are controlled to slowly rise to the requirements of the specific experimental conditions, and the core is left alone for 12 h to keep the core fully saturated with salt water. Then CO_2 was injected into the sand-filled core at a rate of 0.1 mL/min. The injecting is not stopped until CT image acquisition process starts, and CO_2 is continued injected after the image acquisition is completed.

(3) Imbibition process: after the displacement process, salt water saturated with CO_2 is injected into the sand-filled core at an injection rate of 0.1 mL/min, and CT images of the inhalation process are collected in the same way as the displacement process until the inhalation the process is over.

(4) Grayscale image stack acquisition: before injecting salt water, CT continuous scanning is used to obtain the image slice stack of the porous medium saturated with CO_2; then salt water is injected at a constant flow rate, and CT scanning is used to obtain salty water at different pore volume (PV) moments. Change the salt water injection rate, change the porous medium, etc., and repeat the above experiment.

(5) Perform voxel imaging, segmentation and extraction on the obtained gray-scale image stack: According to the image slice stack obtained in step 4, threshold segmentation is performed using the density difference of each phase to obtain the distribution of the phase fluid; quantify the components characterize based on the gray-scale data.

2.3 CT Image Analysis

The processing of the original image mainly includes noise reduction, segmentation and extraction of each phase, and three-dimensional visualization analysis. In order to obtain a clear internal image of the pore, this study used ImageJ and 3D visualization Avizo software to preprocess the original CT image slice stack. Use ImageJ software to crop the image first, leaving the porous medium area only, and then adjust and increase the contrast of the image. The gas phase density is small, so it appears black, and the sandstone density is the largest, and it appears bright white on the grayscale image. The salt water solution with KI added as a contrast agent is somewhere in between, showing off-white.

The experiment uses a calculation method based on CT image parameters. The porosity φ of the filled sandstone core is calculated by the formula (1), where CT_{brine}^{sat} and CT_{CO2}^{sat} are the images of the sand core saturated with salt water and the sand core saturated with CO_2 respectively.CT_{brine} and CT_{CO2} are images of the reactor kettle filled with CO_2 and salt water respectively.

$$\varphi = \frac{CT_{brine}^{sat} - CT_{CO2}^{sat}}{CT_{brine} - CT_{\mathrm{CO2}}} \tag{1}$$

In the same way, during the experiment, CO_2 is injected into the sand-filled sand core saturated with salt water. After reaching the steady state, CT scan was performed to obtain the experimental image CT_{exp}, and then the spatial distribution of CO_2 saturation was calculated using the formula (2):

$$S_g = \frac{CT_{exp} - CT_{CO2}^{sat}}{CT_{CO2}^{sat} - CT_{brine}^{sat}} \tag{2}$$

3 Results and Discussion

3.1 The Influence of Wettability and Heterogeneity

3.1.1 The Influence of Wettability on CO_2 Displacement and Capture Characteristics

Table 2 shows the CO_2 saturation value of each sand-filled layer after the completion of the layered sand-filled core displacement [13]. It can be clearly seen that when the pore structure is similar, the wettability will have a serious impact on the flow and distribution of the CO_2 phase. In the supercritical CO_2 state, when the injection rate is low (0.1 mL/min), the CO_2 phase is stably displaced in the dolomite layer with poor

wettability, occupying most of the pore space of the dolomite layer, and obtaining high CO_2 saturation (0.74). But in the quartz sand layer with strong wettability, there is an obvious capillary fingering phenomenon. CO_2 only displaces a small part of the pores and breaks through, resulting in a lower CO_2 saturation (0.14). As the injection rate increases to 0.3 mL/min, the displacement of CO_2 in the weakly wetted dolomite layer also becomes significantly unstable. CO_2 is unevenly distributed in the pore space of the dolomite, and the saturation drops to 0.55. Further increase (0.6 mL/min), CO_2 in the dolomite layer can almost only flow along the outer pore space, forming a larger finger in the internal pores, and the saturation is further reduced to 0.24. As for the quartz layer, the increase in the injection rate also makes CO_2 trapped in the outer pore space to flow, cannot enter the inner pore space, and the CO_2 saturation is very low. Under the condition of gaseous CO_2, because the viscosity difference between CO_2 and salt water is greater, the displacement process is also more unstable, but the CO_2 saturation (0.29) of the dolomite layer with worse wettability is still greater than that of the strong wettability quartz sand layer (0.12).

Figure 2 shows the dynamic change process of the CO_2 phase in the inhalation process of mixed glass sand and quartz sand. It can be seen from the figure that as the inhalation process progresses, the CO_2 phase will continue to snap off, changing from a continuous phase to an isolated phase. For strongly wetted porous media, capillary fingering is prone to occur in the displacement process, resulting in relatively low CO_2 saturation, but for the inhalation process, strong wettability is conducive to the occurrence of snap off, increasing the safety of C capillary capture and storage. For weakly wettable porous media, the displacement process is more stable and the CO_2 saturation is higher. However, the inhalation process is mainly piston displacement, and CO_2 is difficult to capture, which is not conducive to the safety of CO_2 storage. As for the stratum structure, the structure with strong sealing of the cap layer, the address with poor wettability can be chosen for CO_2 storage, in order to achieve a larger CO_2 storage capacity [6].

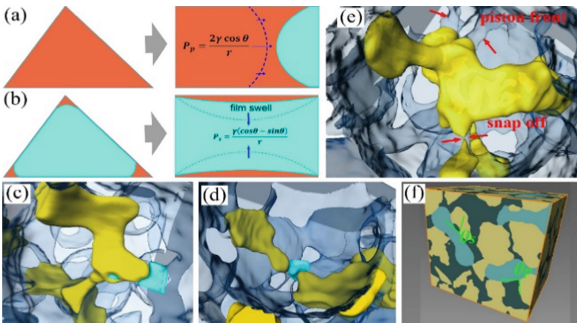

Fig. 2. The piston flooding front and snap-off effect in the pores of glass sand and quartz sand-filled sand cores: (a) The mechanism of the piston flooding front is shown (blue indicates CO_2); (b) CO_2 snap-off mechanism indicates; (c) Piston displacement front occurs (yellow indicates CO_2); (d) CO_2 snap off occurs in the throat; (e) CO_2 piston displacement front edge and snap off occur simultaneously in the throat; (f) The local contact angle when CO_2 is snap-off and the front edge of the piston displacement.

3.1.2 Influence of Heterogeneity on CO_2 Displacement and Capture Characteristics

For structurally heterogeneous cores, at the displacement stage, under supercritical CO_2 conditions, when the injection rate is low (0.1 mL/min), CO_2 first occupies most of the pore space of the BZ06 rock above the core. However, in BZ02 formation with small pores, CO_2 forms two larger branches and develops along the place containing BZ06 sand in the formation. And then it enters BZ06 formation with large pores below the core and occupies most pores, resulting in high CO_2 saturation of BZ06 formation (0.80) and low saturation of BZ02 formation (0.18). In other word, the CO_2 injection rate of the quartz + dolomite layered sand-filled core increases, the CO_2 saturation of both rock layers will decrease. For BZ06 + BZ02 layered sand filling core, with the increase of injection rate, CO_2 saturation is still displaced stably in BZ06 formation, and CO_2 saturation does not decrease (0.81 at 0.3 ml/min injection rate and 0.80 at 0.6 ml/min injection rate). For BZ02 formation, the CO_2 displacement process becomes more unstable, the CO_2 displacement changes from two larger branches to only one displacement path, and the CO_2 saturation decreases to only 0.06 at the injection rate of 0.6 ml/min. Comparing the supercritical CO_2 displacement and gaseous CO_2 displacement processes at the same rate, it is found that the displacement of CO_2 also becomes unstable in the BZ02 rock formation with smaller pores and has no obvious effect on the BZ06 formation. It shows that the changes of injection rate and fluid viscosity mainly affect the rock stratum with small pore structure, but have little effect on the rock stratum with large pores.

During the inhalation process, this experiment found that CO_2, which is the non-wetting phase, also ruptured within a single hole. Analyzing the fractured CO_2 in a single hole, there will be many fractured CO_2 phases in a single hole, and the fractured phases are close to the inner wall of the pore. The shape factor distribution of the fracture phase CO_2 and the comparison of the volume size with the pore volume are calculated. It is found that the shape factors of most isolated CO_2 phases are mainly distributed between 1 and 1.3, and their shape is similar to a sphere (the sphere shape factor is 1), and the volume of almost all fractured isolated CO_2 phases is much smaller than the pore volume. In the mixed glass sand porous medium, there is no obvious CO_2 phase fracture. The main reason for this difference is that the pore structure of the two sand-filled cores is different. Figure 2 shows the comparison of the interface characteristics between the fractured CO_2 phase and the unruptured CO_2 isolated phase. For the CO_2 phase without fracture, the size of the isolated CO_2 phase is relatively large, usually several pores, and there is a part of the contact area between the CO_2 phase and the salt water (medium silver region). When the CO_2 phase ruptures, the isolated CO_2 phase has a smaller volume, generally much smaller than a pore, and the contact area between CO_2 and salt water is also larger.

3.2 Evolution of the Interface Between Phases in the Process of Dissolution and Storage

3.2.1 Types of Phase Interface Evolution

The time-varying CO_2-salt water interface during the salt water imbibition process is shown in Fig. 3, in which only some representative experimental data are shown. *PV*

stands for pore volume (pore volume). In the three-dimensional rendering, each isolated CO_2-salt-water interface is rendered into the corresponding colour according to its size, so as to directly and effectively show the evolution of each isolated interface in the pore.

As CO_2 is gradually split and dissolved by salt water, especially in the later stage of the mass transfer process, only a small amount of CO_2 bubbles occupy the pore space. Therefore, the interface area between the phases is related to the shape of the bubble, but not the same as the surface area of the bubble. The interphase interface with irregular and slender shape can extend to multiple pores, but the monomer area is small. On the contrary, the interphase interface with regular shape and larger area can occupy 2−3 pores. Another phenomenon is that the CO_2-salt water interface is usually located in the void of the pore throat. At this time, CO_2 and salt water are attached to the surface of the porous medium. This type of two-phase bonding will pinch the CO_2-salt-water interface. In order to facilitate effective classification and observation, this chapter divides the CO_2-salt water interface area into three categories based on the data results of all experiments, according to their quantity and area characteristics: interface aggregation nodes, interface clusters and interface monomers.

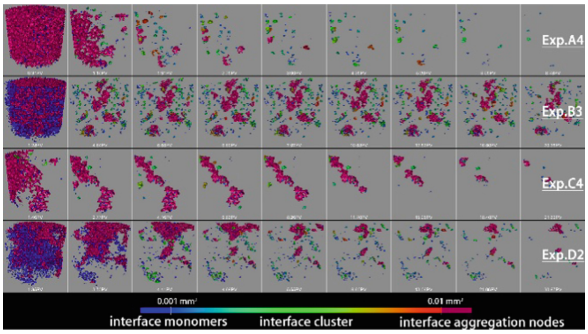

Fig. 3. The time-varying CO_2-salt water interface in the process of salt water absorption

In this study, the interphase interface with an interface area greater than 0.01 mm^2 is called the interface aggregation node, as shown in Fig. 3. The interface aggregation node is composed of interconnected interface clusters, which is significantly larger than other kinds of interphase interfaces, but the number is smaller. During the mass transfer process, the interfacial aggregation nodes further evolved when the salt water invaded, and their number and size decreased. However, more than one interface aggregation node can continue to remain connected and always exist until only a small amount of CO_2 bubbles are left. In Fig. 3, voxels with a color distribution range between red and cyan are classified as interface clusters, and the evolution of the interface is represented by the color gradient. Due to the intrusion of the wetting phase, some parts of the CO_2 phase aggregation node will return from the pore throat to the pores. At this time, the interfacial tension causes the leading part of the non-wetting phase to fragment into interface clusters. The interface between the salt water phases is defined as the interface monomer. For the CO_2 bubbles captured in a single pore, the CO_2-salt water interface is restricted to the pore throat or the corner of the pore. The evolution mode of the

interface monomer does not depend on the flow conditions, but has a certain degree of randomness.

3.2.2 Quantitative Relationship Between Phase Interface Area and Salt Water Saturation

Brusseau [14] conducted air-water displacement and imbibition experiments and found that the air-water phase interface area decreases linearly with the increase of water saturation, which conforms to the linear relationship:

$$a_i = a \times S_w + b \tag{3}$$

Where a_i is the specific interface area, S_w is the salt water saturation, and a and b are constant parameters.

The relationship between specific interface area a_i and salt water saturation S_w under different PV in some experimental groups is shown in Fig. 4, where each data point is calculated from its corresponding two-dimensional slice image, and the solid line represents the linear relationship of each experimental data set Mode. Taking into account a large number of data points (for example, there are more than 2500 points in Exp. D3) and inevitable systematic errors, this strong linear correlation strongly confirms that the specific interface area a_i will vary with the CO_2-salt water two-phase mass transfer process. As the salt water saturation S_w increases, it decreases linearly. During the mass transfer process, the data points of the specific interface area a_i gradually move along the regression line to the zero point, and the distribution range of the data points gradually shrinks.

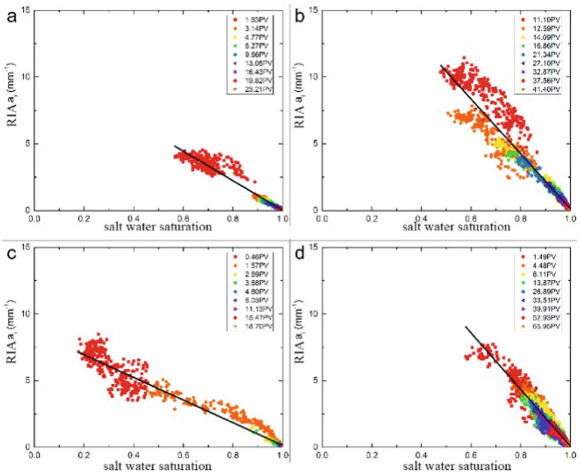

Fig. 4. The relationship between specific interface area and salt water saturation under different PV in some experimental groups.

When quantifying the relationship between the interface area of CO_2-salt water and the degree of salt water saturation, the surface area of the porous media can be

measured, in order to exclude the influence of different porous media particle sizes on the characteristics of the interface area between the phases. According to it, the interface area between CO_2 and salt water is normalized to obtain the relative interface area between CO_2 and salt water, which is recorded as *RIA* (relative interface area). Figure 4 visually shows the linear relationship between relative interface area RIA and salt water saturation. It can be found that for the same salt water saturation, *RIA* of the upward imbibition process is about 1.3 times that of the downward imbibition process. This feature corresponds to Fig. 4. The shape of the interphase interface of the Exp. A experimental group is more irregular, resulting in a larger interphase interface area. As the Reynolds number increases, the slope of the linear relationship in the uniform sand experiment has an increasing trend, while the slope of the linear relationship in the mixed sand experiment is not directly related to the Reynolds number. Under the same Reynolds number, the heterogeneity of the mixed sand significantly increases the contact area of the two phases, so the relative interface area RIA in the mixed sand experiment is larger than that in the uniform sand experiment.

4 Conclusion

This paper uses four sand-filled cores (mixed glass sand, quartz sand, BZ06 + BZ02 layered sand-filled cores and quartz + dolomite layered sand-filled cores) to visualize the CO_2 displacement process and imbibition process under different experimental conditions. In the flow experiment, the microscopic influence mechanism of wettability and heterogeneity on CO_2 displacement and capture characteristics was studied from the pore scale. It is found that during the displacement process, the wettability layered structure and pore layered structure will reduce the permeability of rocks, especially small pore rock formations and strong wettability rock formations, which reduces the storage capacity of CO_2 phase. The increase of the salt water concentration will cause the deterioration of the continuity of the water phase after the displacement process is completed. This phenomenon is more obvious in the strong wettability porous media, and the deterioration of the wettability will reduce the CO_2-salt water phase interface area. During the inhalation process, CO_2 phase rupture was observed, and CO_2 capillary capture was more likely to occur in areas where the wettability or pore structure changed.

The experiment was carried out to measure the area of the CO_2-salt-water interface in homogeneous and heterogeneous sand-filled sand cores, and the evolution of the interface between the phases in the process of dissolution and storage was comprehensively analyzed. The microscopic transport mechanism and morphological distribution characteristics of CO_2-salt water in the pores in this paper has some implication for practical CO_2 long-term and safe storage in saline aquifer.

References

1. Chadwick, R.A., Zweigel, P., Gregersen, U., Kirby, G.A., Holloway, S., Johannessen, P.N.: Geological reservoir characterization of a CO_2 storage site: the Ultra Sand, Sleipner Northern North Sea. Energy **29**(9–10), 1371–1381 (2008)

2. Metz, B., Davidson, O., De Coninck H.: IPCC special report on carbon dioxide capture and storage Working Group III of the Intergovernmental Panel on Climate Change (2005)
3. Niu, B., Al Menhali, A., Krevor, S.C.: The impact of reservoir conditions on the residual trapping of carbon dioxide in Berea sandstone. Water Resour. Res. **51**(4), 2009–2029 (2015)
4. Gao, Y., Qaseminejad Raeini, A., Blunt, M.J., Bijeljic, B.: Pore occupancy, relative permeability and flow intermittency measurements using X-ray micro-tomography in a complex carbonate. Adv. Water Resour. **129**(April), 56–59 (2019)
5. Scanziani, A., et al.: In Situ characterization of three-phase flow in mixed-wet porous media using synchrotron imaging. Water Resour. Res. **56**(9), 1–21 (2020)
6. Wu, B.: Investigation on two-phase flow and mass transfer characteristics of co_2 sequestration in saline aquifer. Dalian University of Technology (Dalian), Dalian (2020)
7. Lv, P.: Pore to core scale influence mechanism of wettability and heterogeneity on co_2 sequestration in saline aquifer. Dalian University of Technology (Dalian), Dalian (2019)
8. Andrew, M., Bijeljic, B., Blunt, M.J.: Pore-scale imaging of trapped supercritical carbon dioxide in sandstones and carbonates. Int. J. Greenh. Gas Control **22**, 1–14 (2014)
9. Chen, C.Y., Horne, R.N., Fourar, M.: Experimental study of liquid-gas flow structure effects on relative permeabilities in a fracture. Water Resour. Res. **40**(8) (2004)
10. George, F.O.: Measurement and estimation of soil water characteristic (April) (2020)
11. Jettestuen, E., Helland, J.O., Prodanovič, M.: A level set method for simulating capillary-controlled displacements at the pore scale with nonzero contact angles. Water Resour. Res. **49**(8), 4645–4661 (2013)
12. Lv, P., et al.: Pore-scale imaging and analysis of phase topologies and displacement mechanisms for co_2-brine two-phase flow in unconsolidated sand packs. Water Resour. Res. **53**(11), 9127–9144 (2019)
13. Jiang, L., Wu, B., Liu, Y., Suekane, T., Wang, D.: Dynamic evolution of the CO_2-brine interfacial area during brine imbibition in porous media. Int. J. Heat Mass Transf. **128**, 1125–1135 (2018)
14. Brusseau, M.L., Peng, S., Schnaar, G., Murao, A.: Measuring air-water interfacial areas with X-ray microtomography and interfacial partitioning tracer tests. Environ. Sci. Technol. **41**(6), 19–1961 (2007)